Progress In Electromagnetics Research Letters, Vol. 104, 67–75, 2022

Design of a Double-Mode Plasmonic Wavelength Filter Using a Defective Circular Nano-Disk Resonator Coupled to Two MIM Waveguides

Imane Zegaar[1], Abdesselam Hocini[2, *], Ahlam Harhouz[2], Djamel Khedrouche[2], and Hocine Ben Salah[3]

Abstract—Various resonance modes, high transmission, and quality factor with simple design are highly desirable parameters for realizing nano-integrated plasmonic devices. In the context, a plasmonic structure consisting of two straight waveguides MIM coupled one central defective circular nano-disk resonator (CNDR) is proposed in this work. The insulator and metal of the proposed plasmonic filter are air and silver, respectively. The plasmonic filter is designed and investigated numerically by using the finite difference time domain method (FDTD). Our simulation results indicate that the proposed plasmonic filter has two transmission peaks with a maximum transmission equal to 80 and 70 percent. The advantages of the proposed filter are the various resonance modes with high transmission peaks and high quality factor which reaches 35.27. In view of these features, our proposed structure of plasmonic filter has the potential to be employed in various devices such as plasmonic demultiplexers and sensors for optical communication purposes.

1. INTRODUCTION

The rapid development of optical communication systems constantly imposes high requirements in terms of transmission speed, capacity, and the size of the elements used, as the traditional optical elements are of large size which is not suitable for application in devices miniaturizations. Plasmonics [1] is a rapidly developing topic that combines fundamental research and applications ranging from various areas such as optical communications [2–4], chemistry [5], biology, and the environmental sciences [6].

Due to their capability to overcome the diffraction limit of light, surface plasmon polaritons (SPPs) are viewed as the most promising alternative for the achievement of highly integrated optical circuits [7, 8]. Surface plasmon polaritons (SPPs) are electromagnetic waves, generated on the metal-dielectric or metal-air interface from the coupling of free electrons with incident photons [9, 10].

As an important plasmonic device, metal-insulator-metal (MIM) waveguide structure has attracted considerable interest due to its capability to provide superior field confinement compared to other structures and its small size. In addition, it can support the propagation of light in the nanoscale regime at the visible and near-infrared ranges [11–13]. All these important advantages of MIM has made it an important factor in attracting the attention of many researchers and designing plasmonic structures. Plasmonic devices-based on MIM waveguides have a wide range of applications in different fields including advanced optical systems [14], chemistry [5], physics [15], and biology [6]. The full-width at half-maximum (FWHM) and Q-factor of resonance wavelength, which determine the performance of the plasmonic filters, are closely dependent on the shape and size of the nanoparticles. Some results

Received 29 January 2022, Accepted 14 April 2022, Scheduled 26 May 2022

* Corresponding author: Abdesselam Hocini (abdesselam.hocini@univ-msila.dz).

[1] Laboratoire d'Ingénierie des Systèmes et Télécommunication Laboratory, University of M'Hamed Bougara Boumerdes, Avenue of Independence, Boumerdes 35000, Algeria. [2] Laboratoire d'Analyse des Signaux et Systèmes, Department of Electronics, University of M'sila, P. O. Box 166, Route Ichebilia, M'sila 28000, Algeria. [3] University Yahia Fares Médéa, Médéa, Algeria.

confirmed that the narrower the line width is, the better the filter performance is. Furthermore, to evaluate the overall performance of the plasmonic sensors figure of merit (FOM) has been proposed which allows nanoparticles to be judged as sensing platforms independent of shape and size [16–18]. Due to useful proprieties of plasmonic structure based on MIM waveguide, previous researches have widely used it for designed optical filter. Zhan et al. proposed a band-pass plasmonic filter based on a nanodisk resonator, and the quality factors of this structure is 25.83 and 28.18 for modes 1 and 2 [19]. Shang et al. designed a plasmonic filter based on a metal-insulator-metal (MIM) waveguide with a stub resonator and a nanodisk resonator, and the Q-factor of this filter for modes 1 and 2 is 11.32 and 14, respectively [20]. Rafiee et al. proposed a multichannel filter based on MIM waveguide coupled multiple split-rings related to T-shape, and the results show that the maximum values for the sensitivity and FOM at six cavities are 1217 nm/RIU and 24.34 [21].

In this study, we propose a novel plasmonic wavelength filter based design consisting of two straight waveguides MIM coupled one central circular nano-disk resonator (CNDR) and including four silver (Ag) defects with the same size and the same distance between them. The effect of the structural parameters on the transmittance properties, the quality factor, refractive index sensitivity, and figure of merit are studied numerically and simulated using FDTD by Rsoft CAD. Based on the results obtained, the proposed device structure could be highly integrated for its transverse size being sub-wavelength-scale.

2. STRUCTURE MODEL AND THEORETICAL ANALYSIS

The schematic of the proposed plasmonic filter is depicted in Figure 1, which consists of two straight waveguides and one central coupled CNDR, including four silver grooves (Ag) with the same size and same inter-distance inserted into the CNDR to generate a defect. The dielectric inside the CNDR and MIM waveguides is air ($n = 1$). Simulations were performed by a 2D FDTD using the software R-SOFT, and the 2D approximation can speed up the simulation time and reduce the required computer resources, without sacrificing the calculation accuracy [22, 23]. The width of the MIM waveguide and the radius of the CNDR are denoted by w and r, respectively. The length and width of the defects are $L1$ and $L2$, respectively. w is the separation among four defects. d is the coupling distance between the circular nano-disk resonator and the waveguide. The upper and lower boundaries are the wave absorption boundaries.

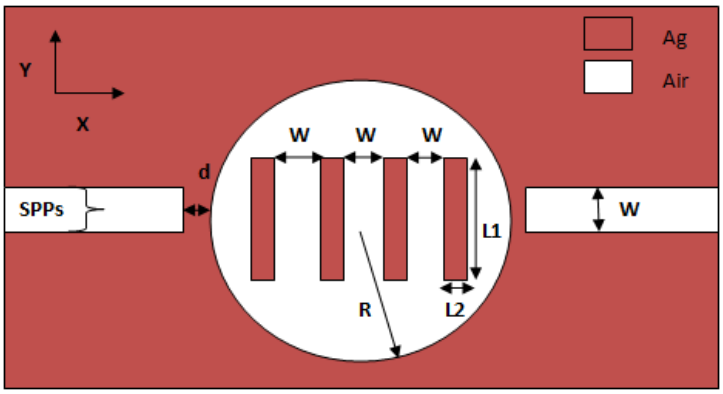

Figure 1. The proposed plasmonic wavelength filter. The geometrical parameters of the proposed structure were set as $w = 50$ nm, $d = 10$ nm, $R = 300$ nm, $L1 = 200$ nm, $L2 = 50$ nm.

The width w of the waveguide is taken as 50 nm so that there is only the fundamental transverse magnetic (TM0) wave excited in this plasmonic system. R, d and s have been maintained at 300, 10, and 50 nm, respectively, and $L1$ and $L2$ are set to 50 nm and 200 nm.

When the incident optical waves transmit through a waveguide, part of the energy will be reflected, and the other part will be coupled into the nanodisk resonator. The resonance condition in nanodisk is

given by [19, 20]:

$$k_d \frac{H_n^{'(1)}(k_m r)}{H_n^{(1)}(k_m r)} = k_m \frac{J_n'(k_d r)}{J_n(k_d r)} \tag{1}$$

where $k_{d,m} = k(\varepsilon_{d,m})^{1/2}$ are the wave vectors in the metal and dielectric nanodisk, respectively, and ε_m and ε_d denote the relative dielectric constant of the metal and dielectric, respectively which can be obtained from the Drude model. k is the wave number; r is the radius of the nanodisk; $H_n^{(1)}$ and $H_n^{'(1)}$ represent the first kind Hankel function of the order n; J_n and J_n' are the first kind Bessel function of the order n and its derivation, respectively.

Accordingly, we model its frequency-dependent complex relative permittivity of silver obtained by Drude model [24]:

$$\varepsilon(\omega) = \varepsilon_\infty - \left(\frac{\omega_p^2}{\omega^2 - i\gamma\omega} \right) \tag{2}$$

where $\varepsilon_\infty = 3.7$ is the dielectric constant at an infinite angular frequency, $\omega_p = 1.38 \times 10^{16}$ Hz the bulk plasma frequency, $\gamma = 2.73 \times 10^{13}$ Hz the damping frequency of oscillations, and ω the angular frequency of the incident wave. The resonance wavelength can be described by:

$$\lambda_m = \frac{2l_{eff}\mathrm{Re}(n_{eff})}{m}, \quad m = 1, 2, 3... \tag{3}$$

l_{eff} is the effective cavity length, and $\mathrm{Re}(n_{eff})$ represents the real part of the effective refractive index. m is the mode number (positive number, i.e., $m = 1$, 2, 3...).

The quality factor is defined as $Q = \frac{\lambda_{res}}{\mathrm{FWHM}}$, where *res* is the resonance wavelength at transmittance peak, and FWHM is the full width at half-maximum of the transmittance spectrum [25].

In this study, the proposed topology is 2D for which the 2D FDTD is used. This is because in other studies for 2D structures such as ours, the 3D results tend to the 2D results, when the structure's length along the y axis increases. To simulate the top and bottom boundaries of our structure, Perfectly Matched Layers (PMLs) are utilized. In both x and z directions, the uniform mesh grid (Δx, Δz) equal to 5 nm was chosen to ensure the rapidity and accuracy of the calculation [26, 27]. Once the incident light of the Gaussian source placed on the left side of the waveguide is TM-polarized wave, the SPPs will be excited, confined, and transmitted in the MIM waveguide.

3. RESULTS AND DISCUSSION

The transmission spectra of the resonator with and without the metallic blocks are numerically calculated by FDTD and are shown in Figure 2. From this figure it can be seen that mode 1 and

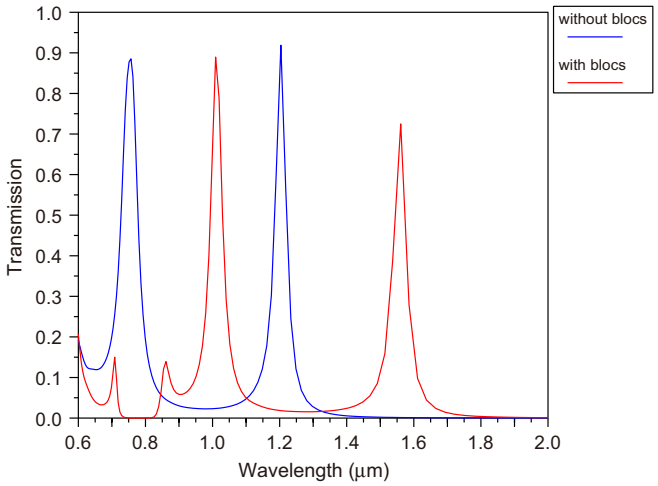

Figure 2. The transmission spectra of the proposed plasmonic filter with and without the metallic blocks.

mode 2 have shifted for larger wavelengths by adding metallic blocks inside the CNDR. Also, the central wavelength of the second mode is adjusted to the optical telecommunication wavelength 1550 nm which resonates at 1200 nm.

Moreover, Figure 3 shows the normal magnetic field distribution (Hy) at four different resonance frequencies, corresponding to the peaks frequencies ($\lambda_{FR1} = 750$ nm and $\lambda_{FR2} = 1200$ nm without blocks, $\lambda_{FR1} = 1010.02$ nm and $\lambda_{FR2} = 1550$ nm with blocks). Resonant light trapping inside the subwavelength CNDR in the form of standing Fabry-Pérot (FP) mode can be seen in Figure 3. It can also be clearly seen that the electromagnetic wave energy was mainly confined in CNDR for the second mode of the structure with blocks. Therefore, this last mode of resonance is more sensitive to the alteration of the refractive index around the surface of distribution, which is very helpful for enhancing the sensitivity if this structure uses such RI sensor.

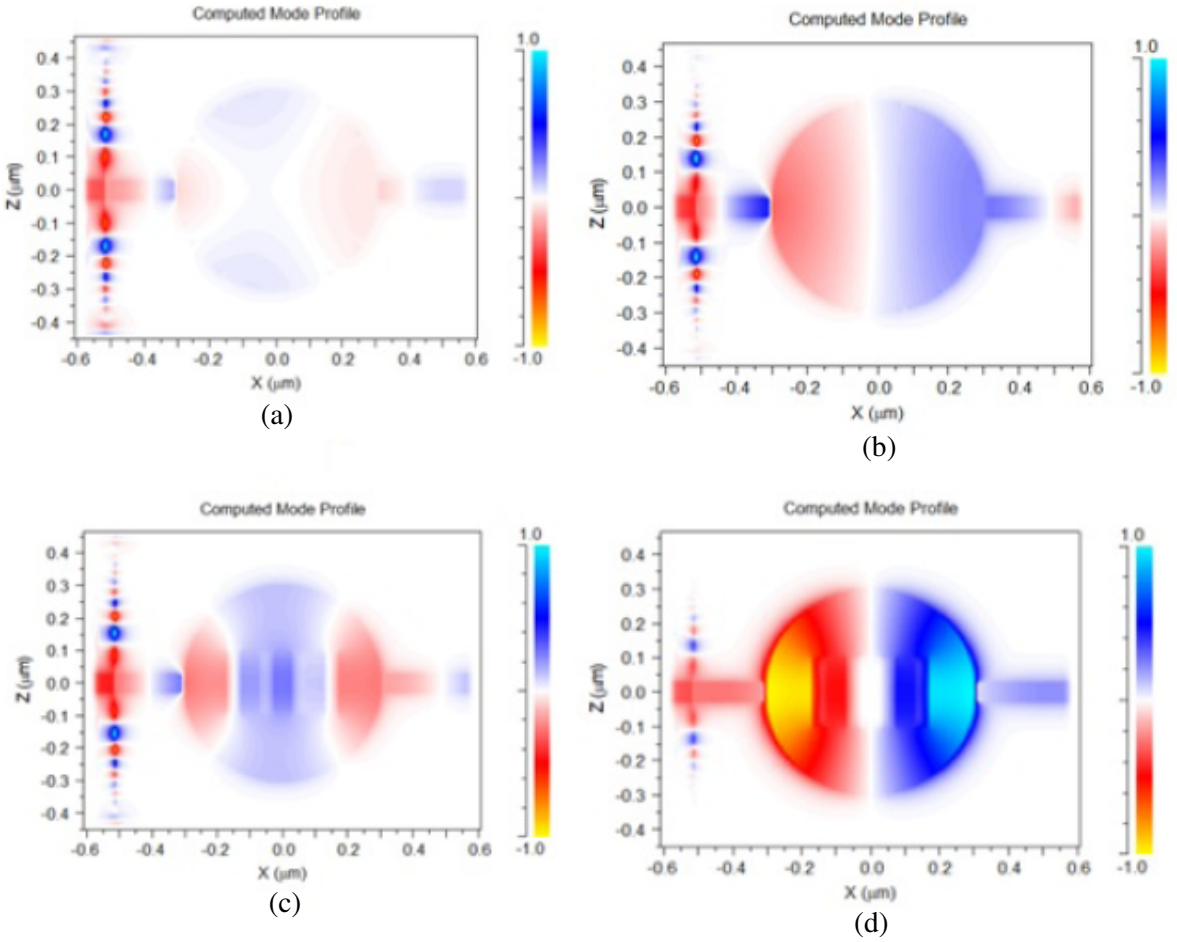

Figure 3. Magnetic field distributions (Hy) at the two resonances wavelengths λ_{FR1} and λ_{FR2}, (a) and (b) without blocks ($\lambda_{FR1} = 750$ nm, $\lambda_{FR2} = 1200$ nm), (c) and (d) with blocks ($\lambda_{FR1} = 1010.02$ nm, $\lambda_{FR2} == 1550$ nm).

In our study, the width and length of the blocks are changed to get insight into the spectral responses, and other parameters are fixed at $d = 10$ nm, $w = 50$ nm, $R = 300$ nm.

At first, in order to make the our designed filter tunable, the effects of the different blocks lengths $L1$ on the wavelength resonance are studied and displayed in Figure 4(a), in which by increasing $L1$, the resonance wavelengths of the two modes shift to the right side. To better view these variations, Figure 4(b) shows the relationship between the maximum transmission peaks and the length of the blocks ($L1$).

Obviously, with increasing the length $L1$ from 190 nm to 220 nm with step 10 nm, the transmission

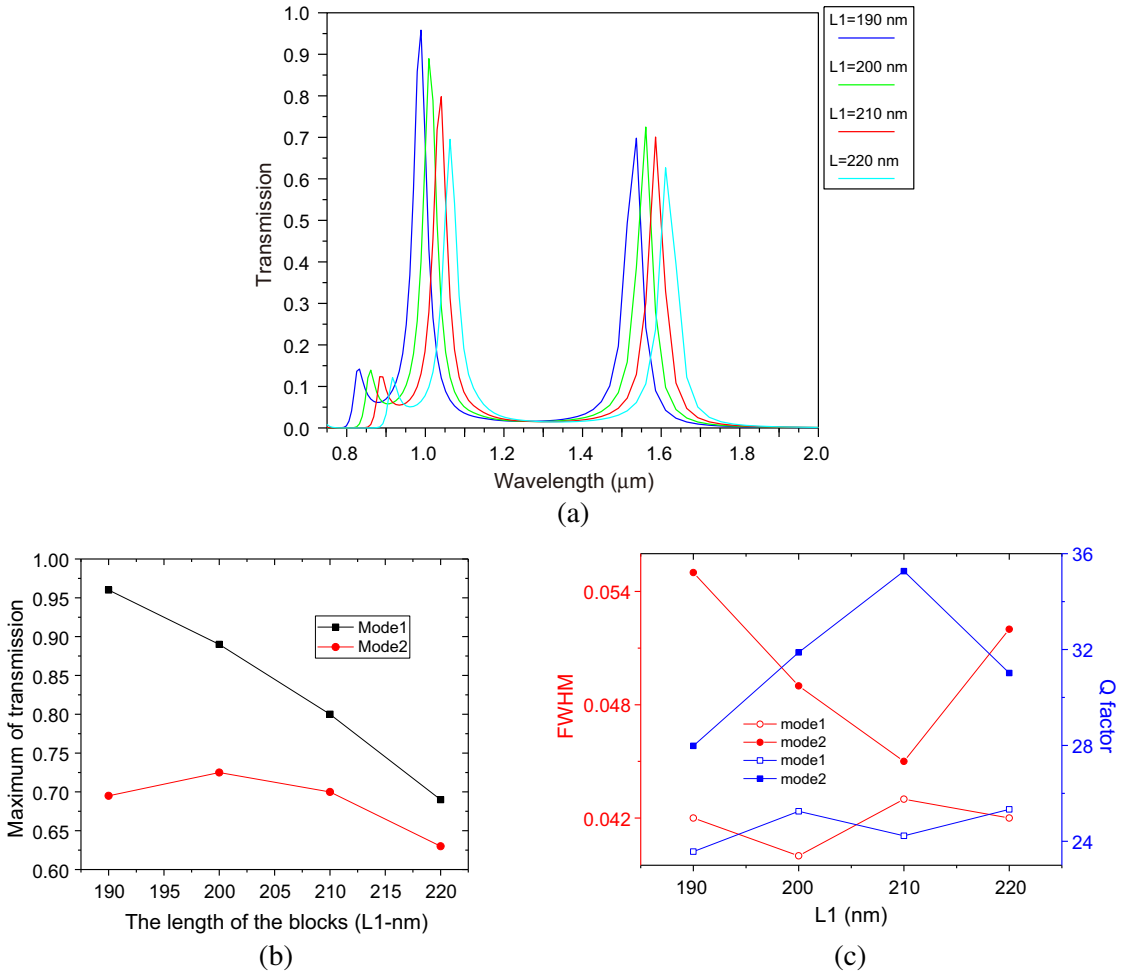

Figure 4. (a) Transmission spectrums for different values of $L1$. (b) Relationship between maximum transmission peaks and different values of $L1$. (c) The full width at half maximum FWHM and Q-factor for different value of $L1$.

spectra of mode 1 significantly decrease compared with mode 2. To find out the best value for $L1$, we calculate the full width at half maximum of the resonance peak (FWHM) and Q-factor at each different value of $L1$. Figure 4(c) shows the full width at half maximum and factor quality respectively of the proposed structure for mode 1 and mode 2 for different values of $L1$, and the result demonstrates that better values of the Q-factor at $L1 = 210$ nm are 24.23 and 35.27 for modes 1 and 2; therefore, the corresponding FWHMs are 0.0436 and 0.0453.

In addition, for different lengths of $L1$, the total undesired transmittance in the region between mode 1 and mode 2 will be adjusted. There is a trade-off between the maximum transmission peaks of two modes and the transmittance level in the stopband region between these modes. Hence, 210 nm has been selected for the $L1$ length. It has almost high quality factor (Q) for mode 2, the lowest FWHM and low transmittance in its stopbands.

From Figure 5(a) with the increase in the block width $L2$, a slight shift is noticed in mode 1, and mode 2 remains at the same wavelength. Moreover, the maximum transmission peak with varied $L2$ stays almost at the same value, and this is in the first and second modes (seen Figure 5(b)). The variation of Q-factor and FWHM for the different values of $L2$ is shown in Figure 5(c), and it is clear that the Q-factor for mode 2, where the width of blocks equals 45 nm and 50 nm, takes the maximum same value which is 35.27, where FWHM = 45 nm to decrease completely at $L2 = 55$ nm. As for mode 1, the value of the Q-factor for the different values of $L1$ is approximately equal to 24, where the value of

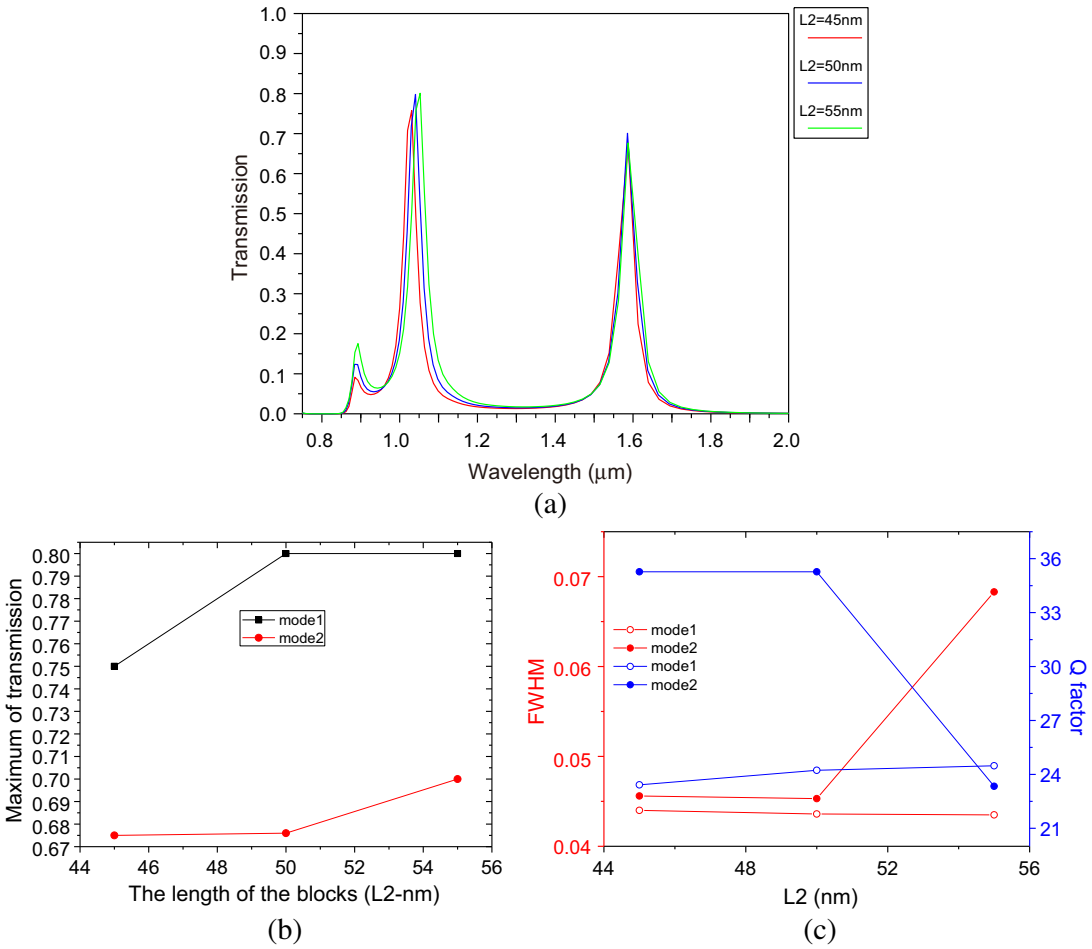

Figure 5. (a) Transmission spectrums for different values of $L2$. (b) Relationship between maximum transmission peaks and different values of $L2$. (c) The full width at half maximum FWHM and Q-factor for different value of $L2$.

FWHM for each $L1$ is almost 43. Also, for various lengths of $L2$, the total undesired transmittance in the region between mode 1 and mode 2 will be adjusted by a slight shift in mode 1.

The trade-off between the maximum transmission peaks of both the modes and the transmittance level in the stopband region between modes 1 and 2 is clear. Hence, 50 nm has been selected for the $L2$ length. It has almost high transmission peaks for mode 1, low transmittance in its stopbands, and high quality factor (Q) for mode 2.

4. APPLICATION PERSPECTIVE

Due to the sharp line-shape and dependency between the resonances wavelengths and the refractive index (RI) of the dielectric material, a high sensitivity and FOM of the spectral response can be obtained by the two modes of resonances with varying the RI of the adjacent medium. The other expression to evaluate the performance of our proposed filter as sensor application is the figure of merit (FOM) and the sensitivity, which can be defined by FOM $= \frac{S}{\text{FWHM}}$, where S is the sensitivity calculated as $S = \frac{\Delta}{\lambda}\Delta n$ nanometer per refractive index (nm/RIU), where $\Delta\lambda$ is the shift of the resonance wavelength of transmittance, and Δn is the refractive index deference.

From Figure 6(a) by increasing the refractive index of $n = 1$ to $n = 1.06$ a shift can be observed in the resonance wavelength despite the $L1$ length variance in the range of 190 to 220 due to the relationship between resonance and refractive indices. The two modes are sensitive to the alteration

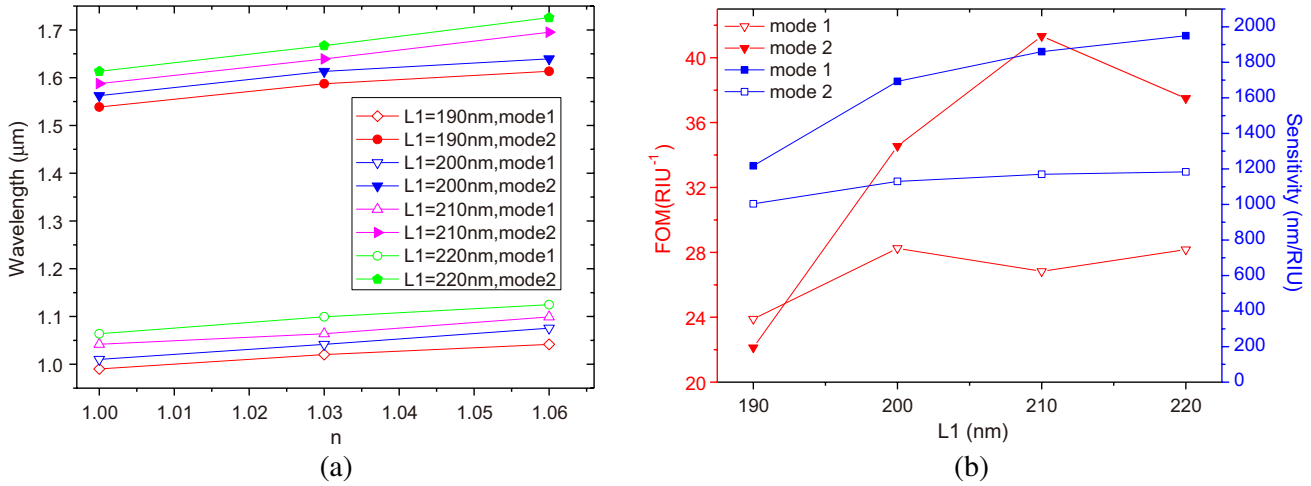

Figure 6. (a) The relationship between the resonance wavelengths and the refractive index with different $L1$. (b) The sensitivity and FOM for different values of $L1$.

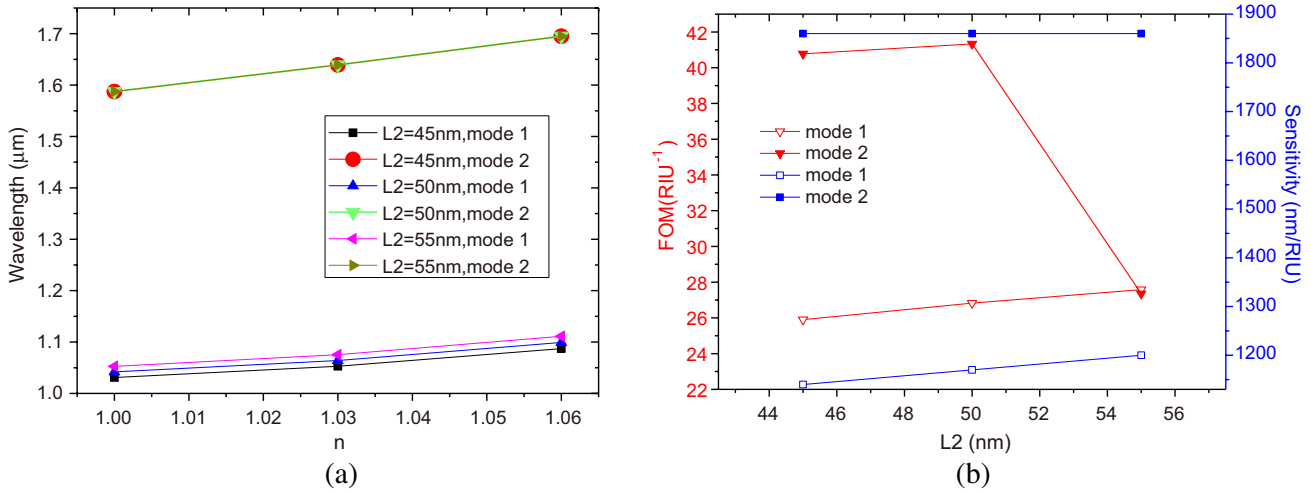

Figure 7. (a) The relationship between the resonance wavelengths and the refractive index with different $L1$. (b) The sensitivity and FOM for different values of $L1$.

of the refractive index around the surface of distribution of the electromagnetic wave energy which is mainly confined in CNDR. Figure 6(b) shows the sensitivities and figure of merit (FOM) of the proposed plasmonic structure for mode 1 and mode 2 with different lengths of the blocks $L1$. Obviously, there is a significant improvement in sensitivity for mode 2 with respect to the length $L1$. A maximum value of 41.33 RIU-1 for the FOM is obtained for mode 2 at $L1 = 210$. Additionally, the sensitivities related to the value of FOM for modes 1 and 2 are 1170 nm/RIU and 1860 nm/RIU, respectively.

Figure 7(a) shows the linear relationship, which is maintained between the resonant wavelengths and the refractive indices of both modes despite the increase in $L2$. Also, the resonance wavelengths for mode 2 of the plasmonic structure taking the same wavelength with the change in length $L2$ with respect to the refractive indices. So they have the same sensitivity value which is 1860 nm (see Figure 7(b)). Further, the optimal value of $L2$ is 50 nm where it has the highest value of FOM. Depending on the sensitivity and FOM value that has been calculated, this filter can be used as a high sensitivity RI sensor.

5. CONCLUSION

In summary, a novel plasmonic wavelength filter is proposed and investigated numerically. This plasmonic filter consists of two straight waveguides MIM coupled one central defective circular nano-disk resonator (CNDR). In the defective circular nano-disk resonator with appropriate parameters, we achieve two resonant wavelengths with high transmittance which can reach 93 percent. The effects of the structural parameters on the transmittance properties are simulated and studied numerically using finite-difference time-domain (FDTD). Our results indicate that the proposed CNDR plasmonic filter has various resonance modes with high transmission peaks, high quality factor, and maximum value of FOM which reach 35.27 and 41.33 RIU^{-1}, respectively. These findings manifest that our design could be applied as an SPP-based filter and has potential applications in nanoscale photonic and integrated optical devices.

REFERENCES

1. Maier, S. A., et al., *Plasmonics: Fundamentals and Applications*, Vol. 1, Springer, 2007.
2. Politano, A., L. Viti, and M. S. Vitiello, "Optoelectronic devices, plasmonics, and photonics with topological insulators," *APL Materials*, Vol. 5, No. 3, 035504, 2017.
3. Wang, L., L. Han, W. Guo, L. Zhang, C. Yao, Z. Chen, Y. Chen, C. Guo, K. Zhang, C.-N. Kuo, et al., "Hybrid dirac semimetal-based photodetector with efficient low-energy photon harvesting," *Light: Science & Applications*, Vol. 11, No. 1, 1–10, 2022.
4. Agarwal, A., M. S. Vitiello, L. Viti, A. Cupolillo, and A. Politano, "Plasmonics with two-dimensional semiconductors: From basic research to technological applications," *Nanoscale*, Vol. 10, No. 19, 8938–8946, 2018.
5. Oliverio, M., S. Perotto, G. C. Messina, L. Lovato, and F. De Angelis, "Chemical functionalization of plasmonic surface biosensors: A tutorial review on issues, strategies, and costs," *ACS Applied Materials & Interfaces*, Vol. 9, No. 35, 29394–29411, 2017.
6. Balbinot, S., A. M. Srivastav, J. Vidic, I. Abdulhalim, and M. Manzano, "Plasmonic biosensors for food control," *Trends in Food Science & Technology*, 2021.
7. Janković, N. and N. Cselyuszka, "High-resolution plasmonic filter and refractive index sensor based on perturbed square cavity with slits and orthogonal feeding scheme," *Plasmonics*, Vol. 14, No. 3, 555–560, 2019.
8. Zhang, Y., S. Li, Z. Chen, P. Jiang, R. Jiao, Y. Zhang, L. Wang, and L. Yu, "Ultra-high sensitivity plasmonic nanosensor based on multiple fano resonance in the MDM side-coupled cavities," *Plasmonics*, Vol. 12, No. 4, 1099–1105, 2017.
9. Shi, L., J. He, C. Tan, Y. Liu, J. Hu, X. Wu, M. Chen, X. Zhang, and S. Zhan, "Plasmonic filter with highly selective wavelength in a fixed dimension based on the loaded rectangular ring cavity," *Optics Communications*, Vol. 439, 125–128, 2019.
10. Butt, M. A., N. L. Kazanskiy, and S. N. Khonina, "Highly integrated plasmonic sensor design for the simultaneous detection of multiple analytes," *Current Applied Physics*, Vol. 20, No. 11, 1274–1280, 2020.
11. Veronis, G. and S. Fan, "Bends and splitters in metal-dielectric-metal subwavelength plasmonic waveguides," *Applied Physics Letters*, Vol. 87, No. 13, 131102, 2005.
12. Lu, H., G. X. Wang, and X. M. Liu, "Manipulation of light in MIM plasmonic waveguide systems," *Chinese Science Bulletin*, Vol. 58, No. 30, 3607–3616, 2013.
13. Diniz, L. O., F. D. Nunes, E. Marega, J. Weiner, and B.-H. V. Borges, "Metal-insulator-metal surface plasmon polariton waveguide filters with cascaded transverse cavities," *Journal of Lightwave Technology*, Vol. 29, No. 5, 714–720, 2010.
14. Rakhshani, M. R. and M. A. Mansouri-Birjandi, "High sensitivity plasmonic refractive index sensing and its application for human blood group identification," *Sensors and Actuators B: Chemical*, Vol. 249, 168–176, 2017.

15. Huang, S., C. Song, G. Zhang, and H. Yan, "Graphene plasmonics: Physics and potential applications," *Nanophotonics*, Vol. 6, No. 6, 1191–1204, 2017.
16. Li, G., X. Chen, O. Li, C. Shao, Y. Jiang, L. Huang, B. Ni, W. Hu, and W. Lu, "A novel plasmonic resonance sensor based on an infrared perfect absorber," *Journal of Physics D: Applied Physics*, Vol. 45, No. 20, 205102, 2012.
17. Ye, J. and P. van Dorpe, "Improvement of figure of merit for gold nanobar array plasmonic sensors," *Plasmonics*, Vol. 6, No. 4, 665–671, 2011.
18. Harhouz, A. and A. Hocini, "Highly sensitive plasmonic temperature sensor based on fano resonances in MIM waveguide coupled with defective oval resonator," *Optical and Quantum Electronics*, Vol. 53, No. 8, 1–11, 2021.
19. Zhan, G., R. Liang, H. Liang, J. Luo, and R. Zhao, "Asymmetric band-pass plasmonic nanodisk filter with mode inhibition and spectrally splitting capabilities," *Optics Express*, Vol. 22, No. 8, 9912–9919, 2014.
20. Shang, C., Z. Chen, L.-L. Wang, Y.-F. Zhao, G.-Y. Duan, and L. Yu, "Characteristics of the coupled-resonator structure based on a stub resonator and a nanodisk resonator," *Chinese Physics Letters*, Vol. 31, No. 11. 114202, 2014.
21. Rafiee, E., R. Negahdari, and F. Emami, "Plasmonic multi channel filter based on split ring resonators: Application to photothermal therapy," *Photonics and Nanostructures-Fundamentals and Applications*, Vol. 33, 21–28, 2019.
22. Chou, Y.-F., C.-T. Chou Chao, H. J. Huang, M. Raziq, and H.-P. Chiang, "Ultrawide bandgap and high sensitivity of a plasmonic metal-insulator-metal waveguide filter with cavity and baffles," *Nanomaterials*, Vol. 10, No. 10, 2030, 2020.
23. Hocini, A., T. Boumaza, M. Bouchemat, F. Royer, D. Jamon, and J. J. Rousseau, "Birefringence in magneto-optical rib waveguides made by Sio_2/Tio_2 doped with γ-Fe_2O_3," *Microelectronics Journal*, Vol. 39, No. 1, 99–102, 2008.
24. Achi, S. E., A. Hocini, H. Ben Salah, and A. Harhouz, "Refractive index sensor MIM based waveguide coupled with a slotted side resonator," *Progress In Electromagnetics Research M*, Vol. 96, 147–156, 2020.
25. Lai, W., K. Wen, J. Lin, Z. Guo, Q. Hu, and Y. Fang, "Plasmonic filter and sensor based on a subwavelength end-coupled hexagonal resonator," *Applied Optics*, Vol. 57, No. 22, 6369–6374, 2018.
26. Ben Salah, H., A. Hocini, M. N. E. Temmar, and D. Khedrouche, "Design of mid infrared high sensitive metal-insulator-metal plasmonic sensor," *Chinese Journal of Physics*, Vol. 61, 86–97, 2019.
27. Hocini, A., D. Khedrouche, N. Melouki, et al., "A high-sensitive sensor and band-stop filter based on intersected double ring resonators in metal-insulator-metal structure," *Optical and Quantum Electronics*, Vol. 52, No. 7, 1–10, 2020.